Electronic Supplementary Information (ESI) for:

Effect of water nanoconfinement on the dynamic properties of paramagnetic colloidal complexes

Luca Bergamasco,[a] Matteo Morciano,[a] and Matteo Fasano[a,*]

[a] Department of Energy, Politecnico di Torino, Corso Duca degli Abruzzi 24, 10129 Torino (Italy)
[*] E-mail: matteo.fasano@polito.it

S1. Detailed Molecular Dynamics (MD) results

Table 1 details the simulated configurations of Gd(DOTA), either bonded to silica wall or in bulk water.

Gd(DOTA) bonded to silica wall

Case	b [nm]	d_{min} [nm]	τ_E [ps]	$\tau_E/\tau_{R,bulk}$ [-]	S^2 [-]	R^2 [-]	T [ns]	Δt [ns]	M [-]	N [-]
1	0.4	0.21	46.2	0.62	0.86	0.84	3.5	2	4	2
2	0.5	0.23	34.6	0.46	0.86	0.85	3.5	2	4	2
3	0.8	0.26	210.5	2.81	0.26	0.94	10	8	3	2
4	1	0.51	149.4	1.99	0.05	0.96	7	4	4	2
5	1	0.36	172.3	2.30	0.06	0.97	7	4	4	2
6	2	1.29	90.3	1.20	0.03	0.99	3.5	2	4	2
7	3	2.00	74.0	0.99	0.02	0.98	3.5	2	4	2

Gd(DOTA) in bulk water

Case	b [nm]	d_{min} [nm]	$\tau_{R,bulk}$ [ps]	S^2 [-]	R^2 [-]	T [ns]	Δt [ns]	M [-]	N [-]
8	-	-	75.0 (300 K)	0.00	0.98	3.5	2	4	2
Exp	-	-	77±4 (298 K)	-	-	-	-	-	-

Table 1 Details of the simulated Gd(DOTA) and/or silica wall setups by means of molecular dynamics simulations. Experimental τ_R of Gd(DOTA) immersed in bulk water is taken from Reference[1], d_{min} is evaluated as the mean minimum normal distance between the silica wall and the Gd(DOTA) atoms during the simulated trajectory, whereas $d = d_{min} + r_{Gd(DOTA)}$, where $r_{Gd(DOTA)} \cong 0.5$nm. Note that R^2 is the coefficient of determination of the Lipari-Szapo fitting, T is the simulation time, Δt is the time span of the RACFs, M is the amount of RACFs evaluated per trajectory, N is the number of trajectories analyzed for the same setup (*i.e.* repetitions), with random initial velocities. For example, in Case 1 RACFs are calculated in the intervals 0–2 ns, 0.5–2.5 ns, 1–3 ns and 1.5–3.5 ns on the two trajectories available.

S2. Simulation convergence
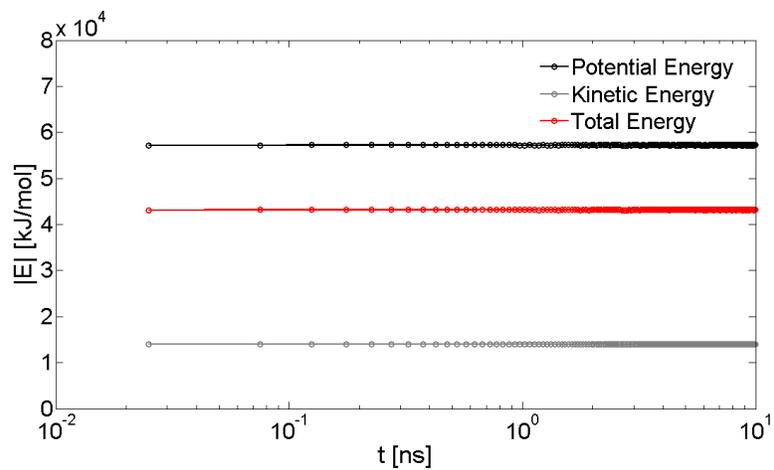
Fig. 1 Energy trends for a Gd(DOTA) complex bonded to silica wall ($d_{min} = 0.26$ nm).
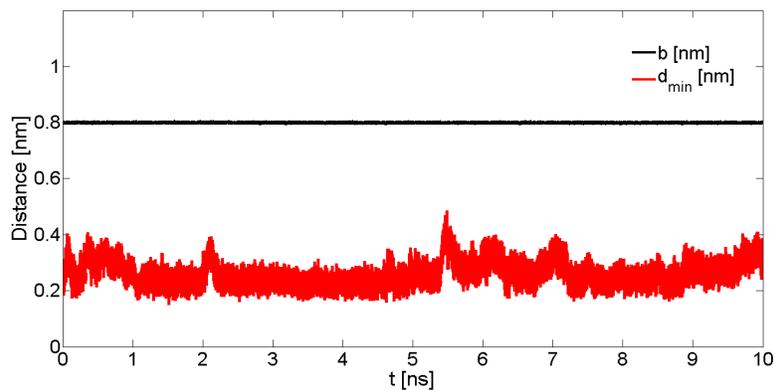
Fig. 2 Trend of the average minimum normal distance d_{min} between silica and Gd(DOTA) atoms during the simulation of a Gd(DOTA) complex bonded to silica wall ($d = 0.76$ nm, $b = 0.80$ nm). The average bond length b between the DOTA compound and silica surface is also shown.

S3. Gd(DOTA) to silica wall distance

The initial relative position of Gd(DOTA) respect to the wall is chosen such that the silica-DOTA bond vector is normal to the silica surface. However, after that the solvated system is equilibrated, Gd(DOTA) is attracted by the silica wall and spontaneously tends to move toward it. Results show that, starting from the initial condition $d_{min} = b$, equilibrium d_{min} is systematically lower than b (in Figure 3 a linear trend is noticeable): Gd(DOTA) molecule approaches the silica wall to minimize the reciprocal nonbonded energy interactions and eventually reach an equilibrium position.
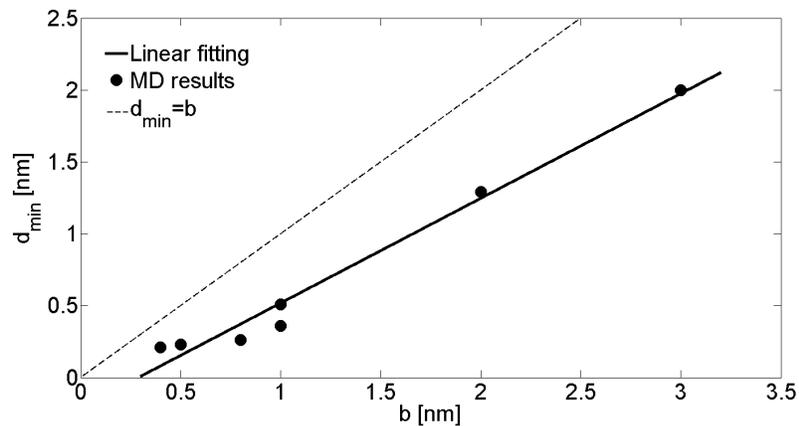
Fig. 3 Relation between the DOTA-silica wall bond length (b) and the average minimum normal distance between Gd(DOTA) atoms and silica wall (d_{min}) in the MD trajectory.

S4. Effective self-diffusivity experienced by Gd(DOTA)
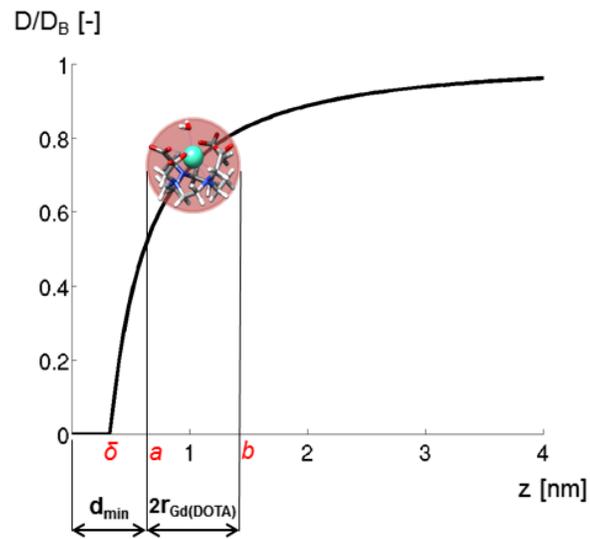
Fig. 4 Schematics for the calculation of the effective self-diffusivity of water experienced by a Gd(DOTA) molecule in the proximity of a silica wall. Note that $d = d_{min} + r_{Gd(DOTA)}$.
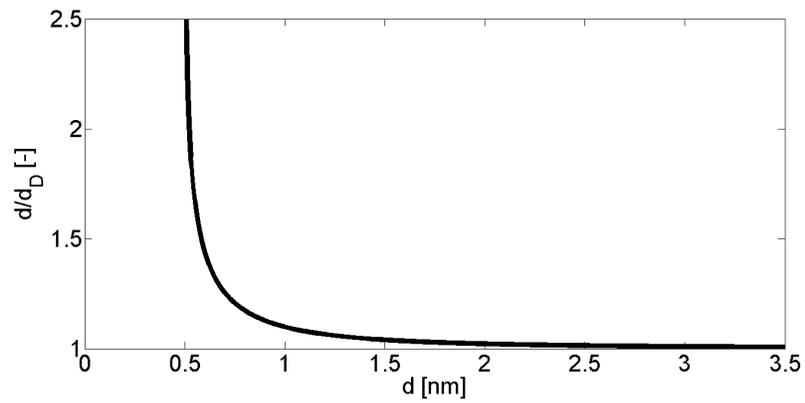
Fig. 5 Increase of the difference between d and d_D distances, while approaching the silica wall surface.

S5. Water nanoconfinement by nanopore or nanoparticle

If water is nanoconfined within a cylindrical nanopore with Φ diameter, the average scaling parameter $\overline{\theta_c}$ of the pore can be expressed as

$$\overline{\theta_c} = 1 - \frac{4\left(\frac{\Phi}{2} - \delta\right)^2}{\Phi^2}. \tag{1}$$

Moreover, by considering the z reference system as normal to the nanopore surface, a local radial value of the scaling parameter $\theta_c(z)$ can be also evaluated:

$$\theta_c(z) = \frac{\frac{\Phi^2}{4} - \left(\frac{\Phi}{2} - \delta\right)^2}{\frac{\Phi^2}{4} - \left(\frac{\Phi}{2} - z\right)^2}. \tag{2}$$

Analogous considerations can be formulated in case of water molecules confined in the proximity of spherical particles with ϕ diameter:

$$\overline{\theta_s} = \frac{\left(\frac{\phi}{2} + \delta\right)^3 - \frac{\phi^3}{8}}{\frac{3}{4\pi}L^3 - \frac{\phi^3}{8}}, \tag{3}$$

where L depends on the particle concentration in the solvent and it is defined as the mean distance between barycenter of contiguous particles; whereas the local scaling parameter is

$$\theta_s(z) = \frac{\left(\frac{\phi}{2} + \delta\right)^3 - \frac{\phi^3}{8}}{\left(\frac{\phi}{2} + z\right)^3 - \frac{\phi^3}{8}}, \tag{4}$$

being z a radial reference system normal to the sphere surface. It is worth to point out that the expressions for the local scaling parameters (namely Equations 2 and 4) are based on geometrical considerations. In detail, these express the ratios between the volumes occupied by the confined water molecules and the volume occupied by the water molecules lying between the solid/liquid interface and a certain radial coordinate. Depending on the case study, the ratio can be expressed for both cylindrical (see Equation 2) and spherical (see Equation 4) geometries.

The effect of either a silica spherical particle (dashed line) or a silica cylindrical pore (solid line) on water nanoconfinement are compared in Figure 6. Both particle and pore have 4 nm radius, while the coordinate reference is chosen such that $z = 0$ nm in correspondence of the particle or pore surfaces. $D(z)$ are evaluated by means of the Equation 12 in the main text, and the characteristic length of nanoconfinement δ is approximately equal to 0.33 nm.[2] In Figure 6a, the ratio between the local radial self-diffusion coefficient of water (D) and the bulk one (D_B) are shown in function of the normal distance from the silica surfaces. Note that a box of pure TIP3P is preliminary simulated as a reference for the bulk properties of water: $D_B = 5.88 \times 10^{-9} \mathrm{m^2 s^{-1}}$ is obtained, in accordance with literature evidences.[3] In Figure 6b, instead, the ratio between local and bulk diffusion times $\tau_D = b_{GdH}^2/D$ of water molecules approaching the silica surface of a particle or pore are represented, where $\tau_{D,bulk} = 17$ ps and the distance of closest approach for the water molecules to the complex is considered as $b_{GdH} = 3.1$ Å.[4] Results show that, at fixed radius, cylindrical geometries intrinsically own larger water confining capabilities than spherical ones. The latter argument can be a first modeling explanation of the different relaxivities measured in case of Gd(DOTA) bonded to spherical or mesoporous particles.[5]
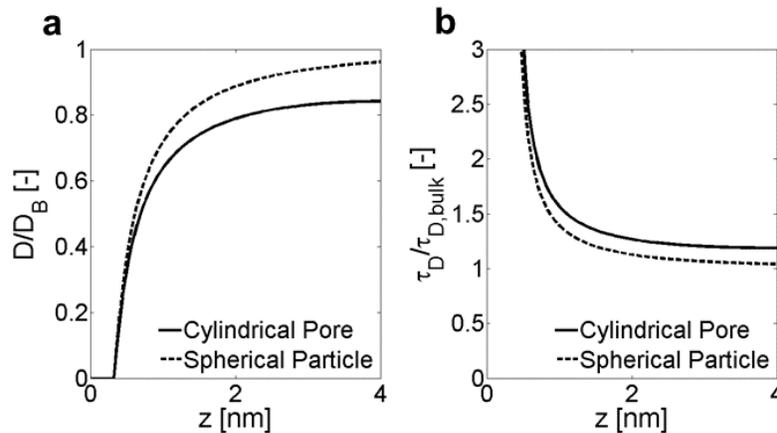
Fig. 6 The effect of a silica spherical particle (dashed line) or a silica cylindrical pore (solid line) on water nanoconfinement are compared based on the scaling law reported in Reference[2]. (a) Ratio between the actual self-diffusion coefficient of water (D) and the bulk one (D_B) as a function of the normal distance z from the silica surfaces. (b) Diffusion times τ_D of water molecules approaching the silica surface of a particle or a pore.

S6. NMRD profiles by SBM model

MRI contrast agents cause an increase in the longitudinal ($1/T_1$) and transverse ($1/T_2$) relaxation rates.[6] The observed solvent relaxation rates are then given by

$$\left(\frac{1}{T_{1,2}}\right)_{obs} = \left(\frac{1}{T_{1,2}}\right)_d + \left(\frac{1}{T_{1,2}}\right)_p, \tag{5}$$

namely a summation of the diamagnetic solvent relaxation rate and a paramagnetic contribution from the contrast agent, which can be in turn expressed in terms of relaxivity:

$$\left(\frac{1}{T_{1,2}}\right)_p = r_{1,2}\, c, \tag{6}$$

where c is the concentration (in mM) of the paramagnetic species.[4] Limiting the analysis to the longitudinal relaxivity, r_1 is given by inner-sphere r_1^{IS} and outer-sphere r_1^{OS} contributions, such that

$$r_1 = r_1^{IS} + r_1^{OS}. \tag{7}$$

While the inner-sphere mechanism is due to the nuclear spin of the water molecules in the first coordination sphere of the metallic ion, water molecules outside this region contribute to the outer-sphere mechanism.[4]

First, the classical theory for estimating the inner-sphere relaxivity has been proposed by Solomon, Bloembergen and Morgan, and it is also known as SBM theory[6]. Thanks to SBM equations, NMRD profiles of MRI contrast agents can be accurately reproduced, at least at magnetic fields of clinical relevance (*i.e.* 0.25–3 T, namely 10–130 MHz). According to SBM theory, longitudinal relaxivity can be expressed as

$$r_1^{IS} = \frac{P_M}{c}\frac{q}{T_{1m} + \tau_m}, \tag{8}$$

where: $P_M \cong m/m_{H20}$ is the mole fraction of metal ions in solution; q is the amount of water in the first coordination sphere of the metal ion; T_{1m} is the relaxation time; τ_m is the residence lifetime of the water proton in the first coordination sphere. T_{1m} can be estimated by SBM equations as:

$$\frac{1}{T_{1m}} = \frac{2}{15}\frac{C_{DD}}{b_{GdH}^6}\left(\frac{7\tau_{c2}}{1+\omega_s^2\tau_{c2}^2} + \frac{3\tau_{c1}}{1+\omega_I^2\tau_{c1}^2}\right) + \frac{2}{3}F(F+1)\left(\frac{A}{\hbar}\right)^2\left(\frac{3\tau_e}{1+\omega_s^2\tau_{c2}^2}\right), \tag{9}$$

where $C_{DD} = \gamma_I^2 g^2 \mu_{B^*}^2 \left(\frac{\mu_0}{4\pi}\right)^2 F(F+1)$ is a constant, $\omega_s = 658\omega_I$ the angular electronic frequency, $\omega_I = \gamma_I B$, B the magnetic field and $\nu_I = \omega_I/2\pi$ the proton Larmor frequency. The correlation times τ_{c1}, τ_{c2} and τ_e can be expressed as:

$$\tau_{ci} = \left(\tau_R^{-1} + \tau_m^{-1} + T_{ie}^{-1}\right)^{-1} \tag{10}$$

$$\tau_e = \left(\tau_m^{-1} + T_{2e}^{-1}\right)^{-1}, \tag{11}$$

where $i = 1, 2$, τ_R is the rotational tumbling time of the contrast agent and

$$\frac{1}{T_{1e}} = \frac{1}{25}\Delta^2\tau_v\left[4F(F+1) - 3\right]\left(\frac{1}{1+\omega_s^2\tau_v^2} + \frac{4}{1+4\omega_s^2\tau_v^2}\right) \tag{12}$$

$$\frac{1}{T_{2e}} = \frac{1}{25}\Delta^2\tau_v\left[4F(F+1) - 3\right]\left(\frac{5}{1+\omega_s^2\tau_v^2} + \frac{2}{1+4\omega_s^2\tau_v^2} + 3\right). \tag{13}$$

In Table 2 the full list of considered physical constants is reported;[4] the definitions of F, A, Δ^2 and τ_v are instead reported in Table 3, together with their typical values in case of Gd(DOTA) contrast agents.

γ_I [T^{-1}s^{-1}]	$2.675 \cdot 10^8$	Gyromagnetic constant for protons
g [-]	2	Electronic g-factor
μ_{B^*} [J T^{-1}]	$9.274 \cdot 10^{-24}$	Bohr magneton
μ_0 [N A^{-2}]	$1.257 \cdot 10^{-6}$	Permeability of vacuum
$\hbar$ [J s]	$1.054 \cdot 10^{-34}$	Reduced Planck constant
N_A [mol^{-1}]	$6.022 \cdot 10^{23}$	Avogadro number

Table 2 Physical constants for SBM equations.

Second, the outer-sphere mechanism of longitudinal relaxivity can be modeled as:

$$r_1^{OS} = \frac{1}{c}\left(\frac{1}{T_1}\right)^{OS} = \left(\frac{32\pi}{405}\right)C_{DD}\frac{N_A}{Dr_{Gd(DOTA)}}Re\left[3j(\omega_I)+7j(\omega_S)\right], \tag{14}$$

being

$$j(\omega) = \frac{\left[4+\left(i\omega\tau_D+\frac{\tau_D}{T_{1e}}\right)^{1/2}\right]}{\left[4+4\left(i\omega\tau_D+\frac{\tau_D}{T_{1e}}\right)^{1/2}+\frac{16}{9}\left(i\omega\tau_D+\frac{\tau_D}{T_{1e}}\right)+\frac{4}{9}\left(i\omega\tau_D+\frac{\tau_D}{T_{1e}}\right)^{3/2}\right]}, \tag{15}$$

$\tau_D = b_{GdH}^2/D_{tot}$ the diffusion time and $D_{tot} = D_{CA}+D \cong D$ the overall diffusion coefficient. In fact, self-diffusivity of water (D) in the proximity of the metallic ion is orders of magnitude larger than the diffusivity of the complex itself D_{CA}.

In the previous formulation of SBM equations, the rotational time of the contrast agent is considered to be isotropic. However, larger or more complex contrast agents may present anisotropic rotation or internal motion, as in the case of Gd(DOTA) molecules chemically bonded to silicon-based large particles. As previously discussed, Lipari and Szabo found that the spectral density function of complex models of motion can be described by two correlation times, which take into account the global (τ_g) and local (τ_l) motion. According to the latter approach, Caravan and colleagues modified the SBM expression for T_{1m} as [7]

$$\begin{aligned}\frac{1}{T_{1m}} &= \frac{2}{15}\frac{C_{DD}}{b_{GdH}^6}\left[\left(S^2\frac{7\tau_{cg2}}{1+\omega_s^2\tau_{cg2}^2}+(1-S^2)\frac{7\tau_{cl2}}{1+\omega_s^2\tau_{cl2}^2}\right)\right.\\ &\quad +\left.\left(S^2\frac{3\tau_{cg1}}{1+\omega_I^2\tau_{cg1}^2}+(1-S^2)\frac{3\tau_{cl1}}{1+\omega_I^2\tau_{cl1}^2}\right)\right]\\ &\quad +\frac{2}{3}F(F+1)\left(\frac{A}{\hbar}\right)^2\left(\frac{3\tau_e}{1+\omega_s^2\tau_{cl2}^2}\right),\end{aligned} \tag{16}$$

where S^2 is the order parameter, while

$$\tau_{cg1,2} = \left(\tau_{R,g}^{-1}+T_{1,2e}^{-1}+\tau_m^{-1}\right)^{-1} \tag{17}$$

$$\tau_{cl1,2} = \left(\tau_{cg1,2}^{-1}+\tau_{R,l}^{-1}\right)^{-1} \tag{18}$$

and $T_{1,2e}$ and τ_e are described by Equations 11, 12 and 13. Note that $\tau_{R,g}$ and $\tau_{R,l}$ are the molecular and local motion of the contrast agent complex, respectively. Clearly, in case of decoupled molecular and local motions ($S^2 = 0$), T_{1m} formulation in Equation 16 reduces to Equation 9. In case of Gd(DOTA) bonded to silicon-based particles, instead, the molecular motion of the complex is described by either SiP or SiMP motion, namely $\tau_{R,g} = \tau_{M,SiP}$ or $\tau_{M,SiMP}^{\perp}$ (see ESI†, S7 for a full calculation of those quantities), whereas the local motion is due to Gd(DOTA), i.e. $\tau_{R,l} = \tau_E$. Note that, for a fair comparison between the MD simulations of this study and the experiments in Reference [5], both the extra correlation time of Gd(DOTA) and the water transport properties obtained from MD simulations and the $D(\theta)$ scaling law at 300 K are linearly scaled to 310 K. In fact, as a first approximation, the classical Stokes-Einstein equation allows to model the relation between water transport properties and temperature as $D \sim T$, at least in the narrow range of ambient temperatures.

S7. Tumbling time of SiP/SiMP particles

Molecular dynamics simulations of a Gd(DOTA) molecule chemically bonded to silica wall, which mimics the surface of a larger silicon nonporous (SiP) or mesoporous particle (SiMP), show that the bulk rotational correlation time of Gd(DOTA) in bulk water is not sufficient to fully describe the overall tumbling motion of complex MRI contrast agents such as those in Reference [5]. Hence, in this section, the tumbling time of micrometer spherical and disk-like particles is estimated by means of Stokes-Einstein relation.

According to Stokes-Einstein's relation for Brownian motion, the rotational diffusion coefficient (D_R) and the molecular correlation time (τ_M) for an isotropic particle are correlated by the classical formula:

$$\tau_M = \frac{1}{6D_R}, \tag{19}$$

where D_R is inversely proportional to the rotational drag coefficient (γ_R), namely

$$D_R = \frac{k_B T}{\gamma_R}, \tag{20}$$

being k_B the Boltzmann constant and T the environment temperature.

In case of spherical particles [4]

$$\gamma_R = 8\mu\pi r_p^3, \tag{21}$$

where μ is the dynamic viscosity of the surrounding media and r_p is the particle radius.

When cylindrical geometries (diameter Φ, length L; axial ratio $p = L/\Phi$) are considered instead, the tumbling ($\tau_M^{\perp}$) and spinning ($\tau_M^{\parallel}$) molecular correlation times are related to the rotational motion transversal or longitudinal to the cylinder length, respectively:

$$\tau_M^{\perp} = \frac{1}{4D_R^{\perp}} \tag{22}$$

$$\tau_M^{\parallel} = \frac{1}{2D_R^{\parallel}}. \tag{23}$$

In case of disk-like particles, rotational diffusion coefficients can be evaluated as [8]:

$$D_R^{\perp} = \frac{1}{6\tau_a} \tag{24}$$

$$D_R^{\parallel} = \frac{1}{\tau_b} - \frac{5}{6\tau_a}, \tag{25}$$

where for $p < 0.75$

$$\begin{aligned} \tau_a &= \tau_0(1.18 + 0.1744(\ln p + 0.2877)^2 - 0.2417(\ln p + 0.2877)^3 + \\ &\quad -3.882 \times 10^{-2}(\ln p + 0.2877)^4) \end{aligned} \tag{26}$$

$$\begin{aligned} \tau_b &= \tau_0(1.183 + 0.2902(\ln p) + 0.4406(\ln p)^2 - 5.850 \times 10^{-2}(\ln p)^3 + \\ &\quad -9.544 \times 10^{-3}(\ln p)^4), \end{aligned} \tag{27}$$

and $\tau_0 = \frac{\pi L^3 \mu}{4p^2 k_B T}$ is the rotational time for a sphere with the same volume of the disk. It is worth to point out that the equations of the rotational times 26 and 27 have been found by interpolating the numerical results obtained by Ortega and co-workers [8].

In the experimental results shown by Gizzatov and colleagues [5], spherical nonporous Silica Particles (SiP) with diameter $\Phi_{SiP} = 1000$ nm and discoidal Silicon Mesoporous Particles (SiMP) with diameter $\Phi_{SiMP} = 1000$ nm and length $L = 400$ nm are analyzed. If bulk conditions are considered for the solvent (*i.e.* dynamic viscosity $\mu \cong 1 \times 10^{-3}$ Pa s at 310 K), Equation 19 implies $\tau_{M,SiP} = 0.13$ s, whereas Equation 22 and 23 $\tau_{M,SiMP}^{\perp} = 0.15$ s and $\tau_{M,SiMP}^{\parallel} = 0.32$ s, respectively.

S8. Gd(DOTA) in bulk water: NMRD profiles by SBM model

Gd(DOTA) in bulk water (Dotarem$^{\copyright}$) is here considered as a representative case for testing the goodness of the implemented SBM equations. Experimental NMRD profiles and parameters are taken from References [4] and [9], and they are fully listed in Table 3. Here, $\tau_R = 53$ ps is considered as the experimental tumbling time of Gd(DOTA) of water at 310 K.[4] Note that Ananta and colleagues demonstrated that this SBM model is calibrated to represent accurately the experimental longitudinal relaxivity of Gd(DOTA) and other gadolinium-based contrast agents, e.g. gadofullerenes and gadonanotubes.[4]

F [-]	7/2	Total electron spin of Gd^{3+}
b_{GdH} [nm]	0.31	Distance between the proton and Gd ion
A [J]	$-3.1 \cdot 10^6$	Hyperfine coupling constant
Δ^2 [s^{-2}]	$30 \cdot 10^{18}$	Mean square zero field splitting energy
τ_v [ps]	7	Correlation time for splitting
τ_m [ns]	122	Water residence time in the inner sphere
τ_D [ns]	40	Diffusion time
$r_{Gd(DOTA)}$ [nm]	0.5	Gd(DOTA) equivalent radius

Table 3 Parameters for SBM equations of Gd(DOTA)-based contrast agents. [4,9]

The comparison of the NMRD profiles, reported in Figure 5 of the main text, show an accurate agreement between the current implementation of the SBM model and the results reported by Ananta and colleagues [4], both in terms of inner sphere contribution and total relaxivity of Dotarem$^{\copyright}$. Longitudinal relaxivity of Gd(DOTA) at clinically relevant conditions ($\nu_I = 60$ MHz, $B = 1.41$ T) is found to be $r_1(1.41 \text{ T}) = 3.2$ mM^{-1}s^{-1}, in good agreement with experimental evidences. [4,9]

S9. Gd(DOTA) bonded to SiMP: NMRD profiles by SBM model

The verified SBM model is then employed to interpret the longitudinal relaxivity of the Gd(DOTA) complexes bounded to silicon particles tested by Gizzatov and colleagues.[5] This analysis takes advantage of the new mechanistic insights from the numerical simulations developed in this work, which allow to correlate some of the parameters required for the SBM model to the relative distance between the bounded Gd(DOTA) and the solid wall (d_{min}). In detail, our simulations demonstrate that water nanoconfinement in the proximity of the solid wall is responsible for the increase in self-diffusion coefficient of water (D), which in turn affects the tumbling motion of bounded Gd(DOTA). The self-diffusivity of nanoconfined water is modelled by the scaling law f_1 previously developed by Chiavazzo and colleagues[2] (see Equation 10 in the main text), whereas the modified tumbling motion of Gd(DOTA) complex bound to solid walls by the new model f_2 presented in the main text as Equations 13–18. These theoretical models generalizing the numerical evidence allow to predict some of the SBM model parameters for the considered configurations with Gd(DOTA) complexes: the diffusion time, *i.e.* $\tau_D = f_1$ (d_{min}), and the tumbling time, *i.e.* $\tau_R = f_2$ (d_{min}) (or, in case of bounded contrast agents, the extra-correlation time $\tau_E = f_2$ (d_{min}) and order parameter $S^2 = f_2$ (d_{min})).

As done for SiP particles in the main text (see Figure 6), here the minimum distance between DOTA and the pore surface of SiMP (d_{min}) is varied over the range 0.22–2 nm, and the corresponding family of NMRD profiles obtained by Equation 16 in case of HP or SP pores are plotted in Figures 7 and 8, respectively. Results show that the observations made for the Gd(DOTA)+SiP case are still valid and the PRE effect evident; however, only negligible differences in the NMRD profiles are noticeable between the Gd(DOTA)+SiP and the Gd(DOTA)+SiMP (both HP and SP) configurations.

The lack of substantial differences in the predicted NMRD profiles of Gd(DOTA)+SiP and Gd(DOTA)+SiMPs contrast agents comes from the comparable molecular motion of SiP and SiMP particles (*i.e.* $\tau_{M,SiP} = 0.13$ s while $\tau_{M,SiMP}^{\perp} = 0.15$ s), the identical τ_E and S^2 trends of Gd(DOTA) in the proximity of both solid surfaces and a similar $\tau_D(z)$ profile (Figure 9). Only slight differences are noticeable between the HP and SP cases, due to the effect of pore curvature on $D(z)$ thus on $\tau_D(z)$ profiles (Figure 9). Note that, while $D(z)$ profiles of local self-diffusivity of water are similar in the HP and SP cases, the average self-diffusivity of water $\overline{D}$ within the pore is significantly different: $\overline{D}/D_B$ increases from 0.70 (SP) to 0.97 (HP) by varying the pore diameter of the SiMP from 5 to 50 nm. Instead, $\overline{D}$ tends to the bulk value for the considered concentration of SiP in the sample, thus the average τ_D reduction may be less pronounced that in the SiMP cases.

Nevertheless, indicatively, in Figure 10 NMRD profiles of Gd(DOTA)+SiP, Gd(DOTA)+SiMP-HP and Gd(DOTA)+SiMP-SP obtained from SBM equations are reported, where d_{min} are optimized for matching the experimental values of r_1 (1.41 T). Model results show that Gd(DOTA)+SiMP-HP should actually present slightly larger d_{min} than Gd(DOTA)+ SiMP-HP (0.28 nm vs. 0.25 nm), whereas Gd(DOTA)+SiMP-SiP should possess the largest d_{min} (0.37 nm).
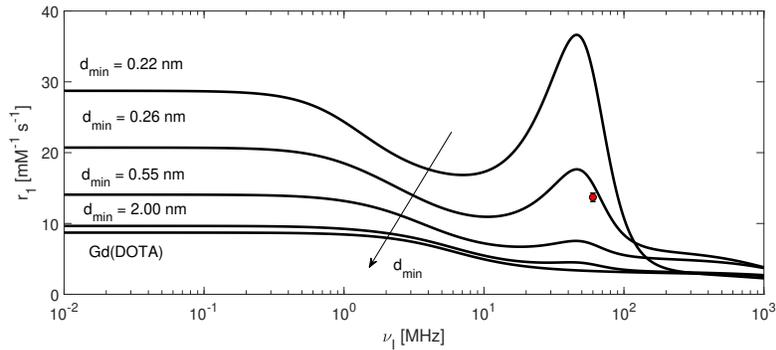
Fig. 7 NMRD profiles of Gd(DOTA) and Gd(DOTA) bonded to the pore surface of SiMP-HP, according to different d_{min}. The latter are obtained from Equation 16. The predicted values of $r_1(1.41 \text{ T})$ at clinically relevant frequencies are the following: 31.3 mM^{-1}s^{-1} ($d_{min} = 0.22$ nm); 15.5 mM^{-1}s^{-1} ($d_{min} = 0.26$ nm); 7.1 mM^{-1}s^{-1} ($d_{min} = 0.55$ nm); 4.2 mM^{-1}s^{-1} ($d_{min} = 2.0$ nm). Note that $r_1(1.41 \text{ T}) = 13.7 \pm 0.6$ mM^{-1}s^{-1} in the experiments, which is represented by the red circle.[5]
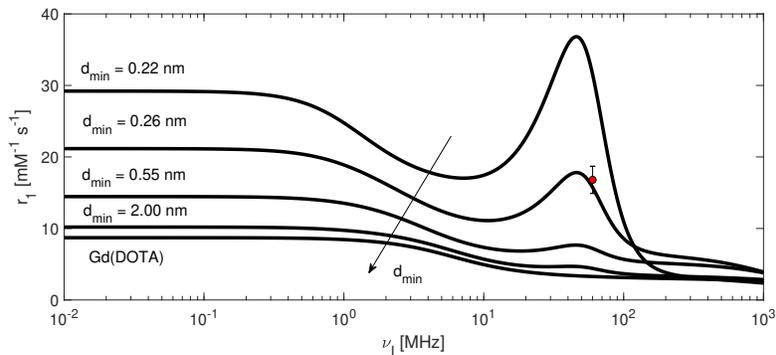
Fig. 8 NMRD profiles of Gd(DOTA) and Gd(DOTA) bonded to the pore surface of SiMP-SP, according to different d_{min}. The latter are obtained from Equation 16. The predicted values of $r_1(1.41\,\text{T})$ at clinically relevant frequencies are the following: $31.5\,\text{mM}^{-1}\text{s}^{-1}$ ($d_{min} = 0.22\,\text{nm}$); $15.7\,\text{mM}^{-1}\text{s}^{-1}$ ($d_{min} = 0.26\,\text{nm}$); $7.2\,\text{mM}^{-1}\text{s}^{-1}$ ($d_{min} = 0.55\,\text{nm}$); $4.4\,\text{mM}^{-1}\text{s}^{-1}$ ($d_{min} = 2.0\,\text{nm}$). Note that $r_1(1.41\,\text{T}) = 16.8 \pm 1.9\,\text{mM}^{-1}\text{s}^{-1}$ in the experiments, which is represented by the red circle.[5]
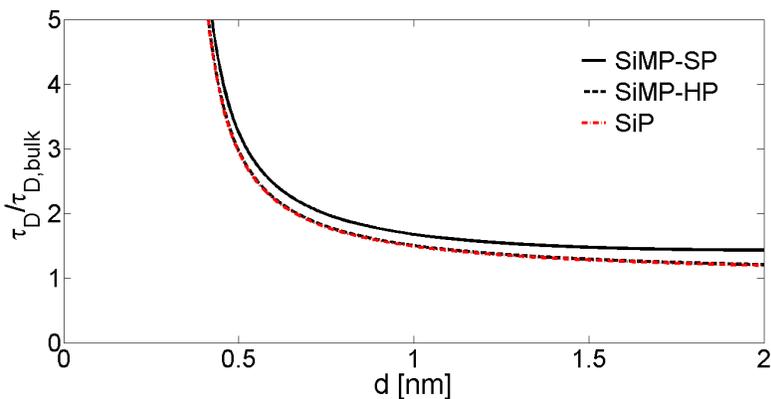
Fig. 9 Ratio between diffusion time of nanoconfined (τ_D) and bulk water ($\tau_{D,bulk}$), with increasing distance d from the solid surface. Results from the scaling law in the ESI†, S5 are shown, where the confining solid interfaces are the SiP surface (dotted red line), the SiMP-SP (solid black line) and SiMP-HP (dotted black line) pore surfaces.
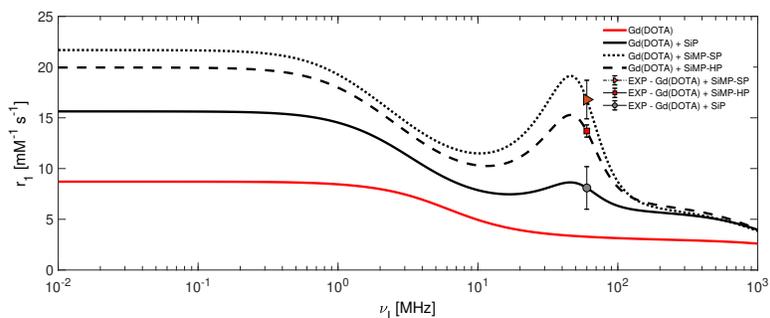
Fig. 10 NMRD profiles for Gd(DOTA) and Gd(DOTA) bonded to the pore surface of SiP, SiMP-SP and SiMP-HP, according to different d_{min}. The predicted values of $r_1(1.41\,\text{T})$ at clinically relevant frequencies reproduce the experimental ones[5], namely: $8.09\,\text{mM}^{-1}\text{s}^{-1}$, which is represented by the gray circle (Gd(DOTA)+SiP, with $d_{min} = 0.37\,\text{nm}$); $16.8\,\text{mM}^{-1}\text{s}^{-1}$, which is represented by the orange triangle (Gd(DOTA)+SiMP-SP, with $d_{min} = 0.25\,\text{nm}$); $13.7\,\text{mM}^{-1}\text{s}^{-1}$, which is represented by the red square (Gd(DOTA)+SiMP-HP, with $d_{min} = 0.28\,\text{nm}$).

S10. Modeling prediction of relaxivity

According to Lauffer[6], three basic strategies exist for reducing the rotational mobility of metal complexes *in vivo* thus enhancing r_1: (i) distribution of the agent into a tissue or tissue compartment with high microviscosity; (ii) non-covalent binding of the complex in tissue to macromolecules; (iii) covalent attachment of the complex to a larger molecule, such as a protein or antibody, before injection.[6] The latter strategy is the so-called PRE method, which exploits the water protons relaxation enhancement induced by the interaction of a low molecular weight complex with a macromolecular substrate.[10] Based on the results obtained from the combination of molecular dynamics data, the scaling law for water self-diffusivity and the SBM model, here we report additional results for the interpretation of the r_1 relaxivity in the light of the PRE method.

Figure 11 shows that an increasing radius of possible Gd-based complexes alternative to DOTA may have a beneficial effect on clinically relevant relaxivities, due to the increased τ_R. Note that, other characteristic relaxation parameters for the resulting Gd-based MRI contrast agents, such as A, Δ^2, τ_v or τ_m, may change with different configurations of the complex (here, for the sake of simplicity, are fixed in all the sensitivity analyses).
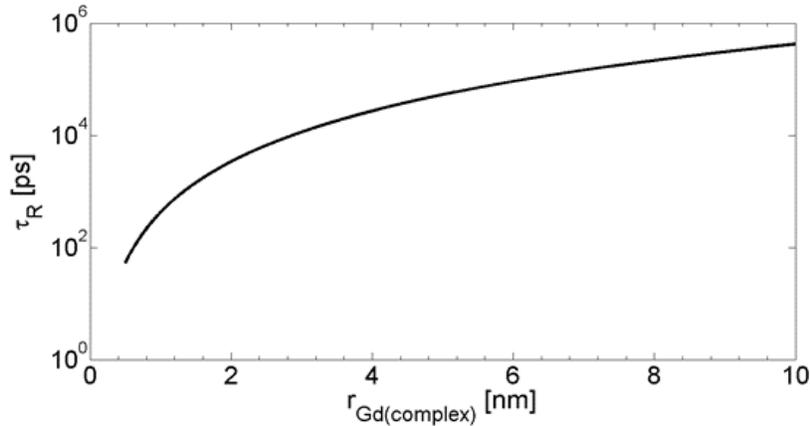
Fig. 11 Tumbling time of Gd-based complexes with increasing radius $\left(r_{Gd(complex)}\right)$.

Figure 12 shows that the relaxivity of Gd(DOTA)+SiP complexes may be enhanced by either increasing the coupling between Gd(DOTA) and SiP motion (*i.e.* $S^2 \to 1$) or by larger SiP diameters. Despite the slight increase in τ_D, and thus r_1^{OS} with Φ_{SiP}, the reported relaxivity enhancement is mainly due to the inner sphere contribution (Figure 13), namely by larger proton relaxation rate $1/T_{1m}$ (Equation 16). While the molecular tumbling time of SiP increases with its diameter ($\tau_{M,SiP} \sim \Phi_{SiP}^3$, as from Equation 19 and Figure 14), a plateau of $1/T_{1m}$ thus r_1^{IS} is reached with $\Phi_{SiP} \cong 4$ nm, thus further increases seem to have no significant effect on r_1.
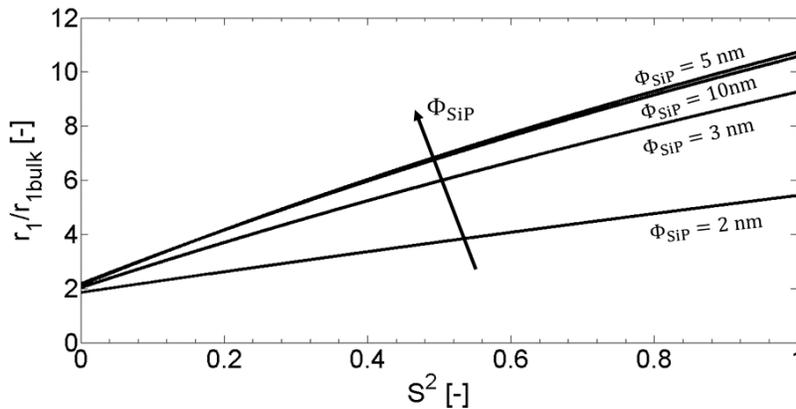
Fig. 12 r_1 (1.41 T) of Gd(DOTA)-SiP complexes with increasing SiP diameter (Φ_{SiP}) and order parameter (S^2), whereas $d_{min} = 0.26$ nm is fixed throughout the cases. Values are normalized by the r_1 (1.41 T) of Gd(DOTA).
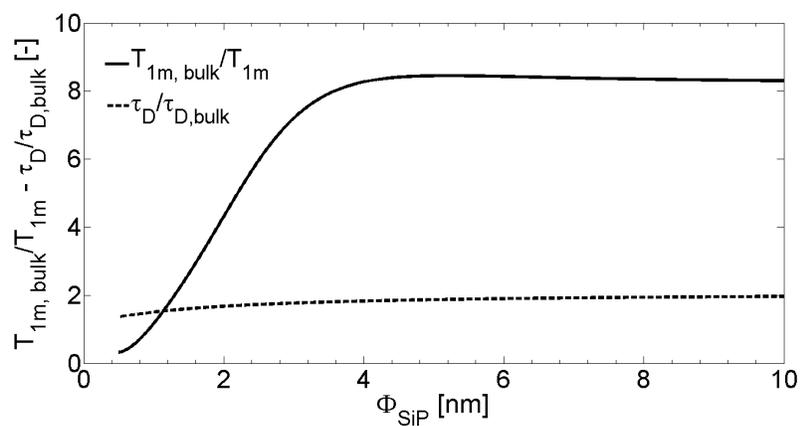
Fig. 13 T_{1m} (solid line) and τ_D (dashed line) at 1.41 T for Gd(DOTA)-SiP complexes with increasing SiP diameter Φ_{SiP}. Values are normalized by the corresponding reference values of Gd(DOTA) immersed in bulk water.
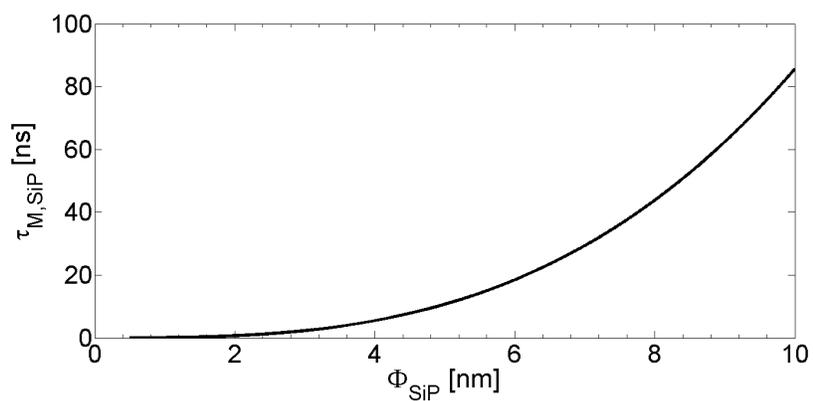
Fig. 14 Molecular tumbling time of SiP with increasing diameter (Φ_{SiP}).

S11. Applicability of the Lipari–Szabo model-free approach

Low fitting accuracy for the Lipari-Szabo model to the computed Rotational Autocorrelation Function – RACF of Gd(DOTA) bonded to the solid wall at the first instants (see Fig. 2b in the main text) could be justified by the effect of bond vibration due to internal energy. To highlight only the intrinsic bond oscillations due to the simulated temperature, we have re-run the simulation 2 ($b = 0.5$ nm, $d_{min} = 0.23$ nm; see Tab. 1) while removing the roto-translational motion of the center of mass of Gd(DOTA). Results in Fig. 15a show that the RACF of the Gd(DOTA) coordination sphere undergoes a fast decorrelation within the first picosecond, followed by a constant value of around 0.995 in the successive instants. This behaviour confirms the fast dynamics of Gd(DOTA) bonds due to internal energy, whose effect vanishes after the first picosecond.

Despite being a dynamic 2 orders of magnitude faster with respect to the effective tumbling motion of Gd(DOTA), it actually affects the accuracy of the adopted Lipari-Szabo model for the first instants of simulation. In Fig. 15b, we compare the best fitting of RACF including the roto-translational motion of the center of mass (solid red line) by: Lipari-Szabo model $C_E(t) = S^2 + (1 - S^2) \exp(-t/\tau_E)$ (black dashed line), and a modified Lipari-Szabo model with equation $C_E(t) = S_A^2 + (A - S^2) \exp(-t/\tau_A)$ (black dotted line), which should take into account the effect of internal energy on bond vibrations. Fitting results show that, while no significant discrepancies are found between the optimised values of the time constants ($\tau_E = 34.6$ ps vs. $\tau_A = 36.8$ ps) and order parameters ($S^2 = 0.86$ vs. $S_A^2 = 0.86$), the modified Lipari-Szabo model achieves a R-square higher than 0.95. Furthermore, the best fitted value of A for this modified model is equal to 0.98, not far from the asymptotic value of RACF shown in Fig. 15a.

Such internal motion of Gd(DOTA) bonds due to internal energy appears anyway to be isotropic and well separable from the tumbling dynamics, thus – as discussed by Andrec and colleagues[11] – it should not compromise the validity of Lipari-Szabo model-free approach to interpret the whole tumbling motion of Gd(DOTA).
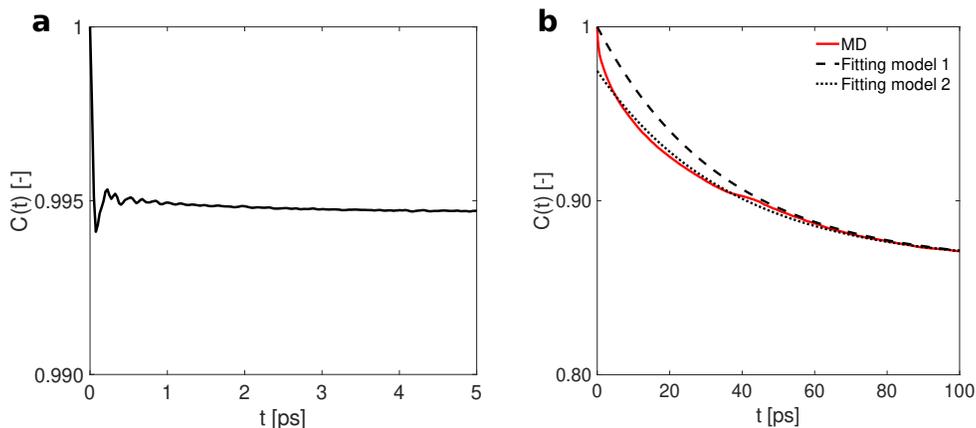
Fig. 15 Effect of internal energy on the bond vibration of the simulated Gd(DOTA) bonded to a silica wall with $d_{min} = 0.23$ nm. (a) RACF of the Gd(DOTA) coordination sphere while removing the roto-translational motion of the center of mass of the molecule. (b) RACF of the Gd(DOTA) coordination sphere (solid red line) fitted by model 1 (black dashed line, *i.e.* Lipari-Szabo model $C_E(t) = S^2 + (1 - S^2) \exp(-t/\tau_E)$ with $S^2 = 0.86$ and $\tau_E = 34.6$ ps) and model 2 (black dotted line, *i.e.* modified Lipari-Szabo model $C_E(t) = S_A^2 + (A - S^2) \exp(-t/\tau_A)$ with $S_A^2 = 0.86$, $\tau_A = 36.8$ ps and $A = 0.98$).

To check also the memoryless dynamics of Gd(DOTA) at short distance from the solid wall, we have compared the characteristic time scales of the autocorrelations for some significant properties of the simulated solvent and Gd(DOTA).

First, both the Velocity (VAF, Fig. 16a) and Momentum (MAF, Fig. 16b) Autocorrelation Functions for the water molecules surrounding the Gd(DOTA) bounded to the silica wall ($b = 0.5$ nm, $d_{min} = 0.23$ nm) result to be completely uncorrelated in a few tenths of picoseconds. Such water dynamics is about 3 orders of magnitude faster than the tumbling motion of Gd(DOTA), thus being well separated between each other.

Second, the Transverse-Current Autocorrelation Function (TCAF) of water in the same bounded Gd(DOTA) configuration has been computed as well. Exploiting the theoretical framework developed by Palmer,[12] it is possible to state that TCAF are related to the dynamic viscosity and thus they are representative of the characteristic time scale of the friction dynamics exerted on the Gd(DOTA). Results in Fig. 17 show that, also in this case, the TCAF of water and the RACF of Gd(DOTA) have more than one order of magnitude time scale separation in their characteristic dynamics. These results are confirmed by previous evidence from the literature.[13,14]

Finally, it is worth to point out that the Lipari-Szabo model-free approach has been applied successfully in many previous studies where the ratio between the size of solvent and tumbling molecules was similar (or even higher) with respect to this case,[15–18] thus remarking a proper separation of time scales between the RACF and the correlation of the friction forces exerted on Gd(DOTA).
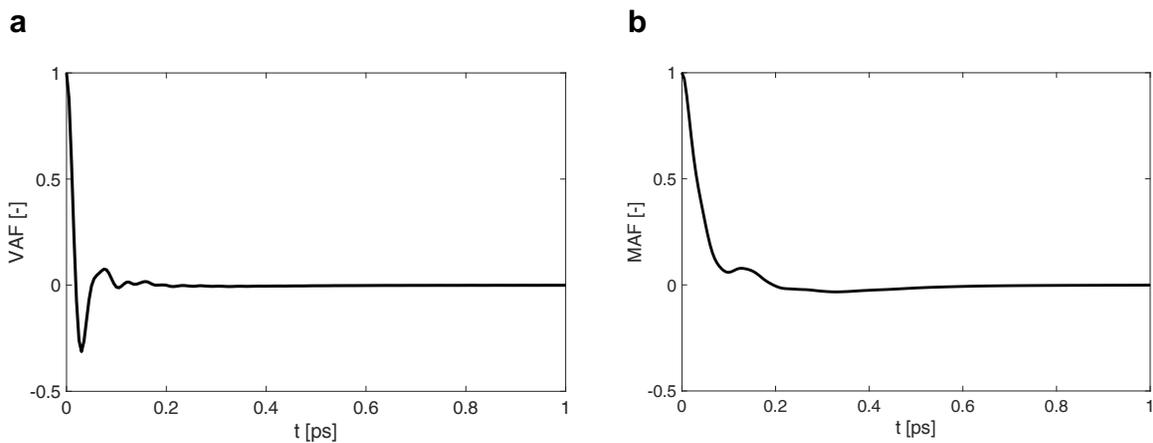
Fig. 16 (a) Velocity Autocorrelation Function – VAF and (b) Momentum Autocorrelation Function – MAF of water molecules surrounding the simulated Gd(DOTA) bonded to a silica wall with $d_{min} = 0.23$ nm.
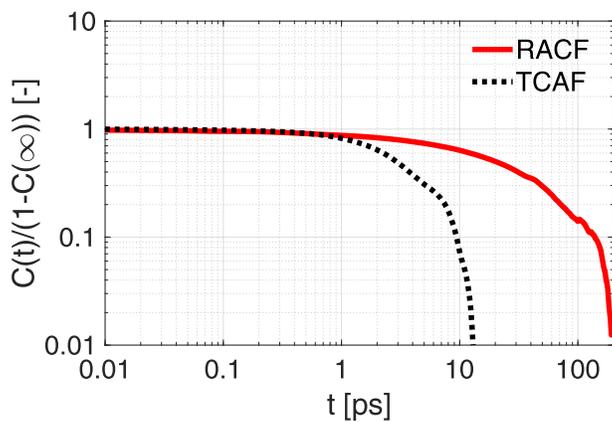
Fig. 17 Comparison between: the Transverse-Current Autocorrelation Function – TCAF of water molecules surrounding the simulated Gd(DOTA) bonded to a silica wall with $d_{min} = 0.23$ nm; the Rotational Autocorrelation Function – RACF of the same Gd(DOTA) coordination sphere. To ease comparability, both ACFs ($C(t)$) have been normalized by $(1 - C(\infty))$, being $C(\infty)$ the value obtained by each ACF for $t \rightarrow \infty$. The TCAF has been averaged over the considered k-vector terms (0.64–5.9 nm^{-1}).

Notes and references

1. D. H. Powell, O. M. N. Dhubhghaill, D. Pubanz, L. Helm, Y. S. Lebedev, W. Schlaepfer and A. E. Merbach, *Journal of the American Chemical Society*, 1996, **118**, 9333–9346.

2. E. Chiavazzo, M. Fasano, P. Asinari and P. Decuzzi, *Nature communications*, 2014, **5**, 4495.

3. P. Mark and L. Nilsson, *The Journal of Physical Chemistry A*, 2001, **105**, 9954–9960.

4. J. S. Ananta, B. Godin, R. Sethi, L. Moriggi, X. Liu, R. E. Serda, R. Krishnamurthy, R. Muthupillai, R. D. Bolskar, L. Helm *et al.*, *Nature nanotechnology*, 2010, **5**, 815–821.

5. A. Gizzatov, C. Stigliano, J. S. Ananta, R. Sethi, R. Xu, A. Guven, M. Ramirez, H. Shen, A. Sood and M. Ferrari, *Cancer letters*, 2014, **352**, 97–101.

6. R. B. Lauffer, *Chemical Reviews*, 1987, **87**, 901–927.

7. P. Caravan, *Chemical Society Reviews*, 2006, **35**, 512–523.

8. A. Ortega and J. G. de la Torre, *The Journal of chemical physics*, 2003, **119**, 9914–9919.

9. S. Laurent, L. V. Elst and R. N. Muller, *Contrast media and molecular imaging*, 2006, **1**, 128–137.

10. P. Caravan, C. T. Farrar, L. Frullano and R. Uppal, *Contrast media and molecular imaging*, 2009, **4**, 89–100.

11. M. Andrec, G. T. Montelione and R. M. Levy, *Journal of Magnetic Resonance*, 1999, **139**, 408–421.

12. B. J. Palmer, *Physical Review E*, 1994, **49**, 359.

13. A. P. Sunda and A. Venkatnathan, *Molecular Simulation*, 2013, **39**, 728–733.

14. B. Hess, *The Journal of chemical physics*, 2002, **116**, 209–217.

15. P. S. Denkova, V. S. Dimitrov, S. M. Bakalova, J. Kaneti and K. Danov, *Magnetic Resonance in Chemistry*, 2003, **41**, 989–995.

16. A. Villa and G. Stock, *Journal of chemical theory and computation*, 2006, **2**, 1228–1236.

17. Y. Yasaka, C. Wakai, N. Matubayasi and M. Nakahara, *The Journal of chemical physics*, 2007, **127**, 104506.

18. Y. Yasaka, M. L. Klein, M. Nakahara and N. Matubayasi, *The Journal of chemical physics*, 2012, **136**, 074508.